HHS Public Access

Author manuscript

Adv Mater. Author manuscript; available in PMC 2020 October 01.

Published in final edited form as:

Adv Mater. 2019 October ; 31(40): e1902956. doi:10.1002/adma.201902956.

Ceria nanoparticles meet hepatic ischemia-reperfusion injury: the perfect imperfection

Dalong Ni[#],
Departments of Radiology and Medical Physics, University of Wisconsin - Madison, Wisconsin 53705, United States

Hao Wei[#],
Departments of Radiology and Medical Physics, University of Wisconsin - Madison, Wisconsin 53705, United States; Department of Nuclear Medicine, Union Hospital, Tongji Medical College, Huazhong University of Science and Technology, Wuhan 430073, China

Weiyu Chen[#],
Departments of Radiology and Medical Physics, University of Wisconsin - Madison, Wisconsin 53705, United States

Qunqun Bao
State Key Laboratory of High Performance Ceramics and Superfine Microstructures, Shanghai Institute of Ceramics, Chinese Academy of Sciences, Shanghai 200050, China

Zachary T. Rosenkrans, **Todd E. Barnhart**, **Carolina A. Ferreira**
Departments of Radiology and Medical Physics, University of Wisconsin - Madison, Wisconsin 53705, United States

Yanpu Wang,
Medical Isotopes Research Center and Department of Radiation Medicine, School of Basic Medical Sciences, Peking University Health Science Center, Beijing 100191, China

Heliang Yao
State Key Laboratory of High Performance Ceramics and Superfine Microstructures, Shanghai Institute of Ceramics, Chinese Academy of Sciences, Shanghai 200050, China

Tuanwei Sun, **Dawei Jiang**, **Shiyong Li**, **Tianye Cao**
Departments of Radiology and Medical Physics, University of Wisconsin - Madison, Wisconsin 53705, United States

Zhaofei Liu,
Medical Isotopes Research Center and Department of Radiation Medicine, School of Basic Medical Sciences, Peking University Health Science Center, Beijing 100191, China

Jonathan W. Engle,

huping@mail.sic.ac.cn, lxl730724@hotmail.com, wcai@uwhealth.org.
Dr. D. Ni, Dr. H. Wei, and Dr. W. Chen contributed equally to this work.

Data availability. The authors declare that the main data supporting the findings of this study are available within the article and its Supplementary Information, which are available from the corresponding authors upon reasonable request.

Competing interests: The authors declare no competing interests.

Departments of Radiology and Medical Physics, University of Wisconsin - Madison, Wisconsin 53705, United States

Ping Hu,
State Key Laboratory of High Performance Ceramics and Superfine Microstructures, Shanghai Institute of Ceramics, Chinese Academy of Sciences, Shanghai 200050, China

Xiaoli Lan,
Department of Nuclear Medicine, Union Hospital, Tongji Medical College, Huazhong University of Science and Technology, Wuhan 430073, China

Weibo Cai
Departments of Radiology and Medical Physics, University of Wisconsin - Madison, Wisconsin 53705, United States; University of Wisconsin Carbone Cancer Center, Madison, Wisconsin 53705, United States

[#] These authors contributed equally to this work.

Abstract

The mononuclear phagocyte system (MPS, e.g., liver and spleen) is often treated as a ‘blackbox’ by nano-researchers in translating nanomedicines. Often, most of the injected nanomaterials are sequestered by the MPS, preventing their delivery to the desired disease areas. Here, we exploit this imperfection by applying nano-antioxidants with preferential liver uptake to directly prevent hepatic ischemia-reperfusion injury (IRI), which is a reactive oxygen species (ROS)-related disease. Ceria nanoparticles (NPs) were selected as a representative nano-antioxidant and detailed mechanism of preventing IRI was investigated. We found that ceria NPs effectively alleviated the clinical symptoms of hepatic IRI by scavenging ROS, inhibiting activation of Kupffer cells and monocyte/macrophage cells. The released pro-inflammatory cytokines were then significantly reduced and the recruitment and infiltration of neutrophils were minimized, which suppressed subsequent inflammatory reaction involved in the liver. The protective effect of nano-antioxidants against hepatic IRI in living animals and the revealed mechanism herein suggests their future use for the treatment of hepatic IRI in the clinic.

Introduction

Hepatic ischemia-reperfusion injury (IRI) has been an important cause of liver damage during surgical procedures such as liver resection, trauma, hypovolemic shock, and liver transplantation, leading to acute liver injury or failure.[1] The hepatic IRI is a multifactorial process that causes up to 10% of early liver failure and improves the incidence of both acute and chronic rejection.[2] Reactive oxygen species (ROS) generated upon re-oxygenation to ischemic tissues is believed to inflict liver damage and initiate a series of deleterious cellular responses including cell death, inflammation, and ultimate hepatic failure.[3] Therefore, ROS is one of the critical targets to prevent hepatic IRI. Anti-oxidative treatment has shown to ameliorate acute liver injury or fibrosis.[4] Although the importance of inhibiting oxidative stress has been recognized for several decades, hepatic IRI remains challenging to treat and there is currently no approved pharmacological intervention in the clinic.[5]

Researchers in fields of nanomedicine and bioengineering have produced nanoscale antioxidants (namely nano-antioxidants) with unique ROS scavenging capability to successfully treat ROS-related diseases including stroke,[6] neurodegenerative diseases,[7] acute kidney injury,[8] atherosclerosis,[9] diabetes,[10] etc. In addition, ROS-responsive delivery systems have been developed.[11] However, translation of nanomedicine for human use has been limited by delivery as most nanomaterials have been nonspecifically uptaken by mononuclear phagocyte systems (MPS, e.g., liver and spleen) to remove them from circulation.[12] Chan and colleagues examined an overall liver clearance mechanism of injected nanomaterials, and found that hard nanomaterials were mainly uptaken and cleared by Kupffer cells and liver sinusoidal endothelial cells.[13] Nano-researchers often treat the accumulation of nanomaterials in the liver/spleen as the biggest hurdle for their clinical translation. However, an exception is when nano-antioxidants are utilized for hepatic IRI - this hurdle is a major benefit and a sufficient dose of nano-antioxidants can be delivered to the liver. Only a few studies have shown the feasibility of antioxidants in the prevention of acute liver injury,[14] and the detailed therapeutic mechanism still remained unknown, which impedes further development of this application.

Among all nano-antioxidants, ceria nanoparticles (NPs) have been widely studied to act as multi-antioxidants for scavenging of ROS, and their detailed mechanism of ROS scavenging have been investigated.[7b, 15] Herein, ceria NPs were selected as a representative and reliable nano-antioxidant to inhibit hepatic IRI. With their ‘blackbox’ of high accumulation in the liver/spleen, our interest is focused on how ceria NPs works *in vivo* to alleviate hepatic IRI. In previous studies, Manne et al. observed that ceria NPs could alleviate the symptoms of hepatic IRI,[16] but neither real-time bio-distribution of ceria NPs *in vivo* nor the detailed mechanism of NPs against IRI involved was studied. Herein, the detailed mechanism of IRI prevention by ceria NPs was investigated in depth, including roles of liver sinusoidal endothelial cells, Kupffer cells and monocyte/macrophage cells, the release of pro-inflammatory cytokines, and the recruitment and infiltration of neutrophils. Our results may provide new perspectives to address the unmet clinical requirement of treating hepatic IRI.

Characterization and ROS scavenging performance of ceria NPs.

Hydrophobic ceria NPs were synthesized *via* a pyrolysis method,[15d] and were transferred to hydrophilic phase through PEGlyation to improve their biocompatibility *in vivo*.[17] The synthesis of ceria NPs were confirmed by transmission electron microscopy (Figure 1b–c), energy dispersive X-ray spectrum (Supplementary Figure 1), and X-ray powder diffraction (Supplementary Figure 2). X-ray photoelectron spectroscopy (XPS) showed that the synthesized ceria NPs contained ~32.01% of cerium(III) oxides and the remaining cerium(IV) oxides (Supplementary Figure 4). Importantly, ceria NPs are reported to possess robust multiple ROS scavenging capability, where the cerium(IV) sites are accountable for the oxidation of H_2O_2 via catalase (CAT)-mimetics while the cerium(III) sites are known to remove $^{\bullet}OH$ and $O_2^{\bullet-}$ via redox reactions or superoxide dismutase (SOD)-mimetics.[18] The ratio of Ce^{3+}/Ce^{4+} in ceria NP in scavenging ROS is important for different ROS-related diseases, and special attention should be paid to the Ce^{3+}/Ce^{4+} composition in ceria NP as well as the reproducibility. Such antioxidative activity of ceria NPs was measured and all

assays confirmed the highly sensitive and concentration-dependent scavenging of ROS by ceria NPs (Figure 1f–h). Electron spin resonance (ESR) spectroscopy further demonstrated the •OH scavenging effect of ceria NPs by using 5,5'-dimethylpyrroline-1-oxide (DMPO) as a spin trapping agent (Figure 1d), where 1:2:2:1 multiple peak in the ESR spectrum showed the presence of •OH and the peaks were sharply decreased upon addition of ceria NPs. In addition, the regenerable ROS scavenging of ceria NPs were evaluated by *in situ* Raman spectroscopy excited with a 488 nm laser. As shown in Figure 1e, major peaks at 460 cm^{-1}, which indicated a symmetric breathing mode of oxygen atoms around Ce,[19] were shifted to new peaks centered at 850/880 cm^{-1} that attributed to the generation of O−O stretching of adsorbed peroxide species on the surface of ceria NPs. An anti-oxidative cycle was found from the generation to disappearance of the adsorbed oxygen species, indicating a recyclable antioxidant capability of ceria NPs. Further *in vitro* experiments showed that high ROS levels in cells destroyed mitochondrial function and led to cell death due to excessive oxidative stress. However, ceria NPs attenuated this response and protected the cells from ROS damage (Supplementary Figure 5–6).

Biodistribution of ceria NPs *in vivo*.

Many types of nanomaterials have been found to accumulate in liver and spleen after intravenous injection, including quantum dots,[13, 20] iron oxide NPs,[17b, 21] and silica NPs.[22] With regard to prevention /treatment of hepatic IRI, this typical 'disadvantageous' liver uptake of nanomaterials is a huge 'advantage' for efficient delivery of agents into the targeted site. Biodistribution of ceria NPs was non-invasively evaluated in real-time via positron emission tomography (PET) imaging. The radionuclide ^{89}Zr was used to label to ceria NPs because Zr^{4+} was found to be easily incorporated within ceria NPs.[15c] As shown in Supplementary Figure 7, the labeling yield increased with temperature and reached 69% at 37 °C and 96% at 55 °C after 2 h of incubation. The ^{89}Zr-ceria NPs were highly stable in both PBS and blood serum as monitored by thin layer chromatography, where more than 85% of ^{89}Zr-ceria NPs remained intact for up to three days (Supplementary Figure 8). Furthermore, PET imaging of mice receiving intravenous (i.v.) injection of ^{89}Zr-ceria NPs was performed to monitor the biodistribution of ^{89}Zr-ceria NPs up to three weeks. As shown from the PET maximum intensity projection images in Figure 2a, dominant blood circulation at 1 h postinjection (p.i.) was found and the blood signal was still obvious at 3 h p.i. This suggests that surface PEGlyation endowed these ceria NPs with excellent circulation. The half-life was calculated to be ~ 2 h (Figure 2b), which is relatively long among inorganic NPs. The liver and spleen were discernable at 3 h p.i. and was the dominant signal from 6 h to 21 days p.i. The ^{89}Zr-ceria NPs showed extremely high *in vivo* stability throughout three weeks as negligible free ^{89}Zr bone and joint uptake was found (free ^{89}Zr was easily absorbed by the bones and joints, Supplementary Figure 9). Quantitative region-of-interest (ROI) analysis of PET images showed that liver uptake of ^{89}Zr-ceria NPs reached a peak at 1 day p.i. (39.5 ± 9.1 %/ID/g, n = 3) and subsequently decreased (Figure 2c), indicating that the NPs was cleared from mouse liver from 1 day up to the 21 day period of the study. *Ex vivo* biodistribution studies corroborated the quantification data from the ROI analysis of PET images (Supplementary Figure 10). Such characteristics of ceria NPs with dominant and long-term accumulation in the liver support their application to combat hepatic IRI *in vivo*.

A system/organ level perspective of the ceria NPs clearance was provided by PET imaging studies shown above. We then proceeded to analyze their biodistribution in the liver on the cellular level. Bio-TEM of liver tissues was performed at 24 h and 7 days p.i. As shown in Figure 2d–e and Supplementary Figure 12, the majority of ceria NPs were located in the lysosomes of the Kupffer-like cells at 24 h and 7 days, which is in accordance with PET imaging results. It is reported that 84.8% of Kupffer cells, 81.5% hepatic B cells, and 64.6% of liver sinusoidal endothelial cells are involved with injected PEGlyated nanomaterials.[13] In hepatic IRI, ROS are mainly released by Kupffer cells or markedly increased in liver sinusoidal endothelial cells.[1c] As the PET imaging and Bio-TEM studies have shown, these ceria NPs are ideal for hepatic IRI therapy since they would likely colocalize with ROS in the Kupffer and liver sinusoidal endothelial cell to directly scavenge them.

Prevention of hepatic IRI with ceria NPs.

The murine model of hepatic IRI was established as previously reported.[23] The protective effects of ceria NPs for IRI were compared between different groups, including a sham-operated group of healthy mice using similar surgical procedure without ligation of the portal triad. The blood samples/liver from all groups were collected and evaluated for liver function at 12 h after surgery. Additionally, the long-term therapeutic assessment of ceria NPs in treated IRI mice at 7 days after the surgery was performed. Aspartate aminotransferase (AST) and alanine aminotransferase (ALT) levels are two common clinical indices for liver health. AST levels from PBS or ceria NPs treated healthy mice were very low, but increased slightly in the sham group (Figure 3a). Significantly elevated AST values was found for IRI mice, which was obviously reduced for ceria NPs treated-IRI group, indicating alleviated tissue injury and overall therapeutic effect of ceria NPs. Any increase of ALT levels is a direct indication of liver injury, whether minor or severe. As shown in Figure 3b, ALT levels for healthy mice with PBS or ceria NPs treatment or sham group were in the normal range, offering the baseline information for liver function. However, significant increase of AST levels was found for PBS-treated IRI mice, but decreased to a much lower value for ceria NPs treated-groups after IRI surgery. All these results demonstrated the hepatic injury in untreated IRI mouse and efficient prevention of IRI by ceria NPs in the treated groups.

Hematoxylin and eosin (H&E) staining of liver tissues was further performed to provide direct evidence of IRI treatment. A large area of severe damage as indicated by the blue dash line in Figure 4c was found in liver section from PBS treated IRI mice along with obvious cytolysis and necrosis of hepatic cells and hemorrhage (marked as yellow oval dashed line). However, only minor damage of liver tissues were observed for ceria NPs-treated IRI group with some structures of lipid droplets (marked as yellow arrows), indicating the protective effect of ceria NPs in preventing IRI. Ceria NPs still play important roles against hepatic IRI at 2 days after surgery (Supplementary Figure 13). Remarkably, no damage was found in the liver of IRI mice at 7 days after treatment of ceria NPs, with histological features similar to healthy mice that received PBS or ceria NPs injection. The liver from mice without treatment may also be healed at 7 days due to the regenerative ability of the liver. Herein, the model of acute liver injury was used to investigate the mechanism of NPs in treating hepatic IRI in the eraly phase when it just started. In the clinic, such intervention is very important

and necessary for patients with hepatic IRI, which could decrease liver damage and extend the time window for surgical procedures. Furthermore, liver profile (including cholesterol, albumin, urea nitrogen, and alkaline phosphatase, Supplementary Figure 14), hematology indices (Supplementary Figure 15–17), and H&E staining of main organs (Supplementary Figure 18) of mice receiving ceria NPs injection within one month demonstrated the excellent biocompatibility of ceria NPs *in vivo*.

Detection of antioxidative indicators in the liver after treatment.

To validate the roles of ceria NPs as antioxidants in IRI mice, we further detailed the antioxidative activity of ceria NPs *in vivo*. As shown in Supplementary Figure S19, dihydroethidium (DHE) staining of liver tissue for superoxide detection indicated that abundant ROS was generated in liver tissues from PBS-treated mice, which was significantly inhibited by treatment with ceria NPs. Liver malondialdehyde (MDA) and 8-hydroxy-2'-deoxyguanosine (8-OHdG) levels are indicators of lipid peroxidation and DNA oxidative damage during hepatic IRI. As shown in Supplementary Figure S20–21, IRI mice receiving injection of ceria NPs had reversed the increased liver MDA and 8-OhdG levels in comparison with those receiving injection of PBS. Both lipid peroxidation and DNA damage of ceria NPs treated mice were similar to those in healthy mice. Superoxide dismutase (SOD) is an important defense to neutralize ROS for cells in the liver, which has been an indicator of oxidative stress. Significantly reduced levels of SOD were found in PBS-treated IRI mice while the SOD levels in ceria NPs treated IRI groups at both 12 h and 7 days p.i. were recovered to similar levels of healthy mice (Supplementary Figure S22). Our results demonstrated that ceria NPs served as reductants to scavenge ROS, inhibited the lipid peroxidation and DNA damage, prevented the depletion of SOD levels, and further protected hepatic cells on IRI mice.

Activation of Kupffer cells and other monocyte/macrophage cells.

The pathophysiology of hepatic IRI involves many mechanisms that each contributes in varying degrees to the overall injury. As demonstrated above, the excessive generation of ROS is clearly recognized as a key mechanism of injury, which is believed to regulate cellular phenotypes during liver reperfusion. To evaluate the effect of cellular phenotypes during treatment of ceria NPs to scavenge ROS, immunofluorescence staining on liver samples was performed by using anti-CLE4F antibody to indicate Kupffer cells (Green), anti-F4/80 antibody to indicate monocyte/macrophage cells (Red), anti-CD31 to indicate endothelial cells (Pink), and DAPI for nuclear staining (Blue). As shown in Figure 5a, healthy mice treated with PBS (A) or ceria NPs (B), and sham group (C) exhibited minimal monocyte/macrophage activation and intact endothelial integrity in the liver. In contrast, hepatic IRI led to significant activation of monocytes/macrophages as well as impaired endothelial integrity (D). As can be seen in Figure 5b, Kuffper and monocyte/macrophage cells were activated to accumulate around and inside the blood vessel, respectively, which is indicated with the dashed yellow oval. Activated Kupffer cells release various products, including cytokines, prostanoids and ROS,[24] which then further activate Kupffer cells in a positive feedback loop that ultimately leads to liver injury. Since ceria NPs scavenge excess ROS, minimal Kupffer and monocyte/macrophages are recruited which preserves the endothelium in liver tissues of ceria NPs treated IRI mice at 12 h (E) and 7 days (F).

Activated monocyte/macrophages and Kupffer cells will significantly increase their release of ROS and pro-inflammatory cytokines. To further demonstrate the activation of monocyte/macrophages and Kupffer cells, we measured several related cytokines in liver tissues from each group, including interleukin-1 (IL-1), interleukin-12 (IL-12), tumor necrosis factor-a (TNF-α), and interferon gamma (INF-γ). As shown in Figure 5a–d, the levels of these pro-inflammatory cytokines were significantly increased for hepatic IRI, and reversed to normal ranges in IRI mice that received ceria NPs treatment. Among them, IL-1 is reported to stimulate the release of ROS by neutrophils, which will further increase TNF-α synthesis by Kupffer cells. As a fundamental role to promote the innate immunity, interleukin-6 (IL-6) is found to be up-regulated by TNF-α, which was further demonstrated in Figure 5e. The nitric oxide synthase 2 (NOS2) is another pro-inflammatory cytokine that produces NO at sustained high levels.[25] NOS2 in the liver from IRI mice was up-regulated (Figure 5f), which suggests overproduction of the highly toxic peroxynitrite anion in combination with additional oxidative stress (mainly superoxide anion). This was ameliorated in IRI mice receiving ceria NPs treatment since they reduce oxidative stress in the liver. Usually, the released pro-inflammatory cytokines further amplify activation of Kupffer cells and promote neutrophil recruitment and adherence to liver sinusoids, which were thoroughly investigated next.

Recruitment and infiltration of neutrophils.

Neutrophils have been well recognized as one of the major effectors during acute injury, which can be recruited to the inflammatory site within minutes.[26] We then evaluated the recruitment of neutrophils and hepatocytes apoptosis by immunofluorescence staining on liver samples. Intracellular adhesion molecule-1 (ICAM-1) is an adhesion molecule of neutrophils, which was stained using an anti-ICAM-1 antibody. As shown in Supplenmentary Figure 25, low ICAM-1 expression was found in liver tissues from healthy mice treated with PBS or ceria NPs and sham group, together with intact endothelial integrity and negligible hepatocytes apoptosis. However, hepatic IRI showed very high expression of ICAM-1, hepatocytes apoptosis, and impaired endothelial integrity. For the ceria NPs-treated group, all these symptoms were ameliorated at 12 h and 7 days after treatment. High expression of the ICAM-1 on the intraluminal side of liver sinusoidal endothelial cells is believed to contribute to the rolling, binding, and parenchymal extravasation of neutrophils.[27] We further evaluated the infiltration of neutrophils using an anti-Ly6G antibody as the neutrophil marker. Figure 4c showed significant neutrophils infiltration for IRI mice receiving PBS treatment, which were clearly observed in zoomed-in images shown below. In comparison, ceria NPs-treated IRI mice exhibited minimal neutrophils infiltration at both 12 h and 7 days after surgery. Myeloperoxidase (MPO) is a heme-containing peroxidase expressed mainly in neutrophils. The recruitment of neutrophils was further demonstrated by significantly higher level of MPO in livers from mice undergoing hepatic IRI (Figure 5g). However, in the liver of ceria NPs-treated IRI mice, MPO was similar to those of healthy mice both at 12 h and 7 days after treatment, corroborating the decreased neutrophil adhesion and infiltration as revealed by immunofluorescence staining.

Mechanism of ceria NPs to prevent hepatic IRI.

Small amounts of ROS produced during oxidative metabolism in healthy livers are tolerated without any apparent side effects. However, when such a process is aberrant, excess ROS generated from both intracellular and extracellular sources during re-oxygenation to ischemic tissues may lead to hepatic IRI. Taken together the experimental results shown above, we propose the following mechanism for the prevention of hepatic IRI by ceria NPs (Scheme 1). First, ceria NPs were primarily uptaken by the MPS system (liver and spleen), largely in the liver sinusoidal endothelial cells and Kupffer cells. ROS generated from both intracellular and extracellular location during the IRI process were efficiently scavenged by ceria NPs that restored SOD levels and alleviated lipid peroxidation/DNA damage. The activation of Kupffer cells and monocyte/macrophage cells during IRI was significantly inhibited with less release of pro-inflammatory cytokines as well as the restricted adhesion of neutrophils. Therefore, the recruitment and infiltration of neutrophils during hepatic IRI was successfully inhibited with ceria NPs, which reduces the subsequent inflammatory response involved.[26] Since different nano-antixoidants showed similar ROS-scavenging performance and most of them were accumulated in the liver after intravenous injection, we believed our study will also shine light on their potential use as nano-antixoidants for preventing hepatic IRI.

Conclusion

We presented here the treatment of hepatic IRI in living animals by utilizing the ‘blackbox’ effect of nanomaterials (i.e., liver uptake). Importantly, the detailed mechanism for nano-antioxidants in preventing IRI has been proposed based on our results from the detailed experimental studies. Such mechanism may also minimize hepatic IRI in patients who may receive a liver transplant with distribution of ceria NPs.[5] Future work is required to investigate whether the described mechanism can be applied to other kinds of nano-antioxidants such as inorganic manganese NPs or organic carbon and melanin NPs.[6, 28] On the basis of our findings, the *in vivo* fate of these nano-antioxidants after preventing IRI adds another interesting facet to promote their quick clearance from the liver after treatment. As demonstrated by Chan et al., altering both macrophage phenotype and hepatic sinusoidal blood velocity are two new strategies to affect liver sequestration and clearance of nanomaterials and the relevant technologies are currently available,[13] which required in-depth investigation in future. Overall, this study provides a detailed glimpse into the nano-antioxidants against hepatic IRI, which will also offer a foundation for future studies to treat other IRI caused by general surgery or liver diseases with therapeutic nanomaterials.

Supplementary Material

Refer to Web version on PubMed Central for supplementary material.

Acknowledgments

This work was supported, in part, by the University of Wisconsin – Madison and the National Institutes of Health (P30CA014520), the National Natural Science Foundation of China (NO. 81471712, NO. 81671747), the Key Project of National Natural Science Foundation of China (No. 81630049). Shanghai Science and Technology Rising Star Project (NO. 19QA1410100), and Youth Innovation Promotion Association CAS (NO. 20190218).

Reference

[1]. a)Eltzschig HK, Eckle T, Nat. Med 2011, 17, 1391; [PubMed: 22064429] b)Monga SP, Nat. Med 2018, 24, 6; [PubMed: 29315298] c)Peralta C, Jimenez-Castro MB, Gracia-Sancho J, J. Hepatol 2013, 59, 1094. [PubMed: 23811302]

[2]. Howard TK, Klintmalm G, Cofer JB, Husberg BS, Goldstein RM, Gonwa TA, Transplantation 1990, 49, 103. [PubMed: 2300999]

[3]. a)Alban FT, Gyamfi D, van Golen RF, Heger M, in The Liver, Elsevier, 2018, 79;b)Bhogal RH, Weston CJ, Velduis S, GD Leuvenink H, Reynolds GM, Davies S, Nyguet-Thin L, Alfaifi M, Shepard EL, Boteon Y, Liver Transpl 2018, 24, 1437; [PubMed: 30040176] c)Fondevila C, Busuttil RW, Kupiec-Weglinski JW, Exp. Mol. Pathol 2003, 74, 86; [PubMed: 12710939] d)Jaeschke H, Chem. Biol. Interact 1991, 79, 115. [PubMed: 1884426]

[4]. a)Selzner N, Rudiger H, Graf R, Clavien P-A, Gastroenterology 2003, 125, 917; [PubMed: 12949736] b)He SQ, Zhang YH, Venugopal SK, Dicus CW, Perez RV, Ramsamooj R, Nantz MH, Zern MA, Wu J, Liver Transpl 2006, 12, 1869; [PubMed: 17133584] c)Chouchani ET, Pell VR, Gaude E, Aksentijevic D, Sundier SY, Robb EL, Logan A, Nadtochiy SM, Ord ENJ, Smith AC, Eyassu F, Shirley R, Hu CH, Dare AJ, James AM, Rogatti S, Hartley RC, Eaton S, Costa ASH, Brookes PS, Davidson SM, Duchen MR, Saeb-Parsy K, Shattock MJ, Robinson AJ, Work LM, Frezza C, Krieg T, Murphy MP, Nature 2014, 515, 431. [PubMed: 25383517]

[5]. Zhai Y, Petrowsky H, Hong JC, Busuttil RW, Kupiec-Weglinski JW, Nat. Rev. Gastroenterol Hepatol 2013, 10, 79. [PubMed: 23229329]

[6]. a)Liu Y, Ai K, Ji X, Askhatova D, Du R, Lu L, Shi J, J. Am. Chem. Soc 2017, 139, 856; [PubMed: 27997170] b)Lee HJ, Park J, Yoon OJ, Kim HW, Lee DY, Kim DH, Lee WB, Lee NE, Bonventre JV, Kim SS, Nat. Nanotechnol 2011, 6, 121. [PubMed: 21278749]

[7]. a)Kwon HJ, Cha MY, Kim D, Kim DK, Soh M, Shin K, Hyeon T, Mook-Jung I, ACS Nano 2016, 10, 2860; [PubMed: 26844592] b)Kwon HJ, Kim D, Seo K, Kim YG, Han SI, Kang T, Soh M, Hyeon T, Angew. Chem. Int. Ed 2018, 57, 9408.

[8]. a)Ni D, Jiang D, Kutyreff CJ, Lai J, Yan Y, Barnhart TE, Yu B, Im HJ, Kang L, Cho SY, Liu Z, Huang P, Engle JW, Cai W, Nat. Commun 2018, 9, 5421; [PubMed: 30575745] b)Jiang D, Ge Z, Im H-J, England CG, Ni D, Hou J, Zhang L, Kutyreff CJ, Yan Y, Liu Y, Cho SY, Engle JW, Shi J, Huang P, Fan C, Yan H, Cai W, Nat. Biomed. Eng 2018, 2, 865. [PubMed: 30505626]

[9]. Wang Y, Li L, Zhao W, Dou Y, An H, Tao H, Xu X, Jia Y, Lu S, Zhang J, Hu H, ACS Nano 2018, 12, 8943. [PubMed: 30114351]

[10]. a)Jahani M, Shokrzadeh M, Vafaei-Pour Z, Zamani E, Shaki F, Asian J Anim. Vet. Adv 2016, 11, 226;b)Dkhil M, Zrieq R, Al-Quraishy S, Abdel Moneim A, Molecules 2016, 21, 1517.

[11]. a)Lu Y, Aimetti AA, Langer R, Gu Z, Nat. Rev. Mater 2016, 2, 16075;b)Wang J, Zhang Y, Archibong E, Ligler FS, Gu Z, Adv. Biosyst 2017, 1, 1700084.

[12]. a)Bourquin J, Milosevic A, Hauser D, Lehner R, Blank F, Petri-Fink A, Rothen-Rutishauser B, Adv. Mater 2018, 30, e1704307; [PubMed: 29389049] b)Feliu N, Docter D, Heine M, del Pino P, Ashraf S, Kolosnjaj-Tabi J, Macchiarini P, Nielsen P, Alloyeau D, Gazeau F, Stauber RH, Parak WJ, Chem. Soc. Rev 2016, 45, 2440. [PubMed: 26862602]

[13]. Tsoi KM, MacParland SA, Ma XZ, Spetzler VN, Echeverri J, Ouyang B, Fadel SM, Sykes EA, Goldaracena N, Kaths JM, Conneely JB, Alman BA, Selzner M, Ostrowski MA, Adeyi OA, Zilman A, McGilvray ID, Chan WC, Nat. Mater 2016, 15, 1212. [PubMed: 27525571]

[14]. a)Bao QY, Geng DD, Xue JW, Zhou G, Gu SY, Ding Y, Zhang C, Int. J. Pharm 2013, 446, 112; [PubMed: 23416166] b)Wu J, Liu L, Yen RD, Catana A, Nantz MH, Zern MA, Hepatology 2004, 40, 195. [PubMed: 15239103]

[15]. a)Chen J, Patil S, Seal S, McGinnis JF, Nat. Nanotechnol 2006, 1, 142; [PubMed: 18654167] b)Kim CK, Kim T, Choi IY, Soh M, Kim D, Kim YJ, Jang H, Yang HS, Kim JY, Park HK, Park SP, Park S, Yu T, Yoon BW, Lee SH, Hyeon T, Angew. Chem. Int. Ed 2012, 51, 11039;c)Soh M, Kang DW, Jeong HG, Kim D, Kim DY, Yang W, Song C, Baik S, Choi IY, Ki SK, Kwon HJ, Kim T, Kim CK, Lee SH, Hyeon T, Angew. Chem. Int. Ed 2017, 56, 11399;d)Bao Q, Hu P, Xu Y, Cheng T, Wei C, Pan L, Shi J, ACS Nano 2018, 12, 6794. [PubMed: 29932327]

[16]. Manne N, Arvapalli R, Graffeo VA, Bandarupalli VVK, Shokuhfar T, Patel S, Rice KM, Ginjupalli GK, Blough ER, Cell. Physiol. Biochem 2017, 42, 1837. [PubMed: 28750366]

[17]. a)Li LL, Zhang R, Yin L, Zheng K, Qin W, Selvin PR, Lu Y, Angew. Chem. Int. Ed 2012, 51, 6121;b)Ni D, Ferreira CA, Barnhart TE, Quach V, Yu B, Jiang D, Wei W, Liu H, Engle JW, Hu P, Cai W, J. Am. Chem. Soc 2018, 140, 14971. [PubMed: 30336003]

[18]. a)Korsvik C, Patil S, Seal S, Self WT, Chem. Commun 2007, 1056;b)Xue Y, Luan Q, Yang D, Yao X, Zhou K, J. Phys. Chem. C 2011, 115, 4433;c)Pirmohamed T, Dowding JM, Singh S, Wasserman B, Heckert E, Karakoti AS, King JE, Seal S, Self WT, Chem. Commun 2010, 46, 2736.

[19]. Wang YJ, Dong H, Lyu GM, Zhang HY, Ke J, Kang LQ, Teng JL, Sun LD, Si R, Zhang J, Liu YJ, Zhang YW, Huang YH, Yan CH, Nanoscale 2015, 7, 13981. [PubMed: 26228305]

[20]. Ye L, Yong K-T, Liu L, Roy I, Hu R, Zhu J, Cai H, Law W-C, Liu J, Wang K, Liu J, Liu Y, Hu Y, Zhang X, Swihart MT, Prasad PN, Nat. Nanotechnol 2012, 7, 453. [PubMed: 22609691]

[21]. Lee JH, Huh YM, Jun YW, Seo JW, Jang JT, Song HT, Kim S, Cho EJ, Yoon HG, Suh JS, Cheon J, Nat. Med 2007, 13, 95. [PubMed: 17187073]

[22]. a)Chen F, Goel S, Valdovinos HF, Luo H, Hernandez R, Barnhart TE, Cai W, ACS Nano 2015, 9, 7950; [PubMed: 26213260] b)Ni D, Jiang D, Ehlerding EB, Huang P, Cai W, ACC. Chem. Res 2018, 51, 778. [PubMed: 29489335]

[23]. Tsung A, Sahai R, Tanaka H, Nakao A, Fink MP, Lotze MT, Yang H, Li J, Tracey KJ, Geller DA, Billiar TR, J. Exp. Med 2005, 201, 1135. [PubMed: 15795240]

[24]. Bilzer M, Roggel F, Gerbes AL, Liver Int 2006, 26, 1175. [PubMed: 17105582]

[25]. Coleman JW, Int. Immunopharmacol 2001, 1, 1397. [PubMed: 11515807]

[26]. Kolaczkowska E, Kubes P, Nat. Rev. Immunol 2013, 13, 159. [PubMed: 23435331]

[27]. Perry BC, Soltys D, Toledo AH, Toledo-Pereyra LH, J. Invest. Surg 2011, 24, 178. [PubMed: 21675854]

[28]. a)Lucente-Schultz RM, Moore VC, Leonard AD, Price BK, Kosynkin DV, Lu M, Partha R, Conyers JL, Tour JM, J. Am. Chem. Soc 2009, 131, 3934; [PubMed: 19243186] b)Li W, Liu Z, Liu C, Guan Y, Ren J, Qu X, Angew. Chem. Int. Ed 2017, 56, 13661.

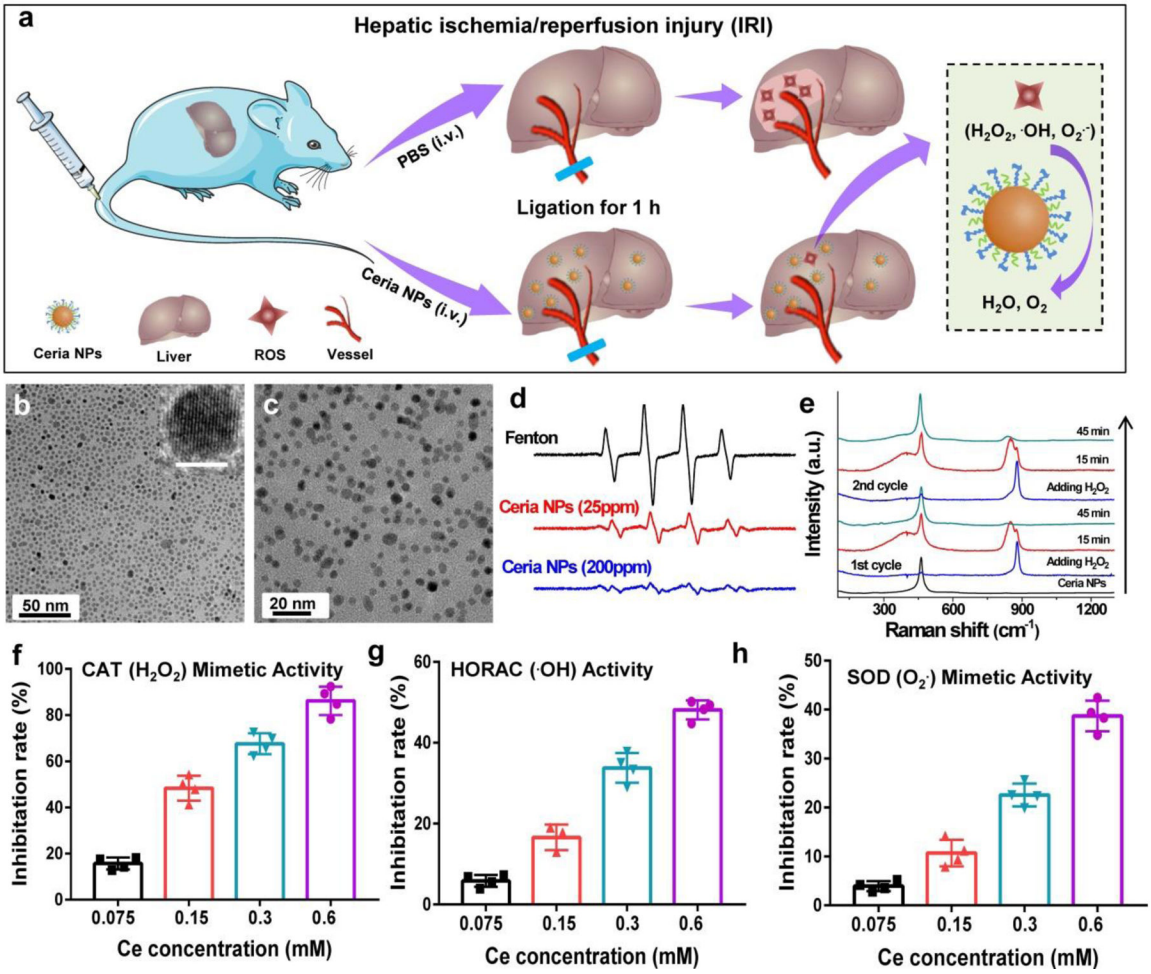

Figure 1. A schematic treatment of IRI using ceria NPs and their ROS scavenging performance.

a Schematic illustration of preventing IRI by ceria NPs. TEM images of ceria NPs before (**b**) and after PEGlyation (**c**). Scale bar inset: 5 nm. **d**. ESR spectra of the different group using DMPO as a spin trap agent. **e**. Raman spectra of ceria NPs reacting with H_2O_2 at varied time points within 45 min in each cycle. ROS scavenging activity of ceria NPs mimics catalase (CAT, **f**), SOD (**h**) and eliminate •OH (**g**). In **f-h**, data represent means ± s.d. from four independent replicates.

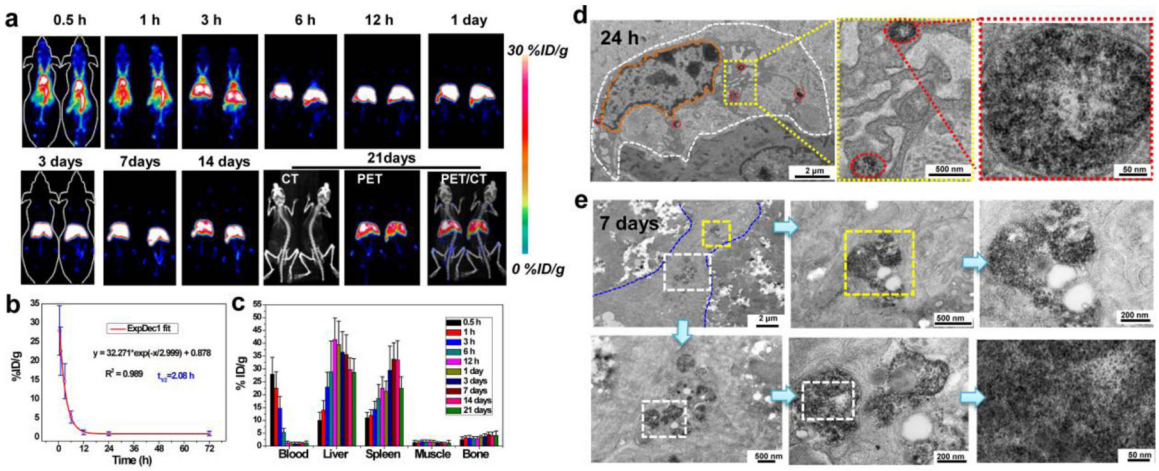

Figure 2. Biodistribution of ceria NPs *in vivo*.

a Representative maximum intensity projection PET images of mice at various time points after i.v. injection of ^{89}Zr-ceria NPs. **b** Time-activity curve of ^{89}Zr-ceria NPs in the blood. **c** Quantification of ^{89}Zr-ceria NPs uptake in the blood, liver, spleen, muscle, and bone at various time points p.i.. Bio-TEM images of mouse liver sinusoid showing the presence of NPs in the liver at 24 h (**d**) or 7 days (**e**) after i.v. injection of ceria NPs. White dashed line in (**d**) highlights the outline of Kupffer-like cells, while the orange dashed line within indicates the nucleus of Kuffper-like cells and red dash ovals showed the endocytosis of ceria NPs by lysosome. Blue dashed line in (**e**) highlights other cut direction of Kupffer-like cells and the white or yellow dashed rectangles showed the enlarged portion of the images. In **a**-**c**, data represent means ± s.d. from three independent replicates.

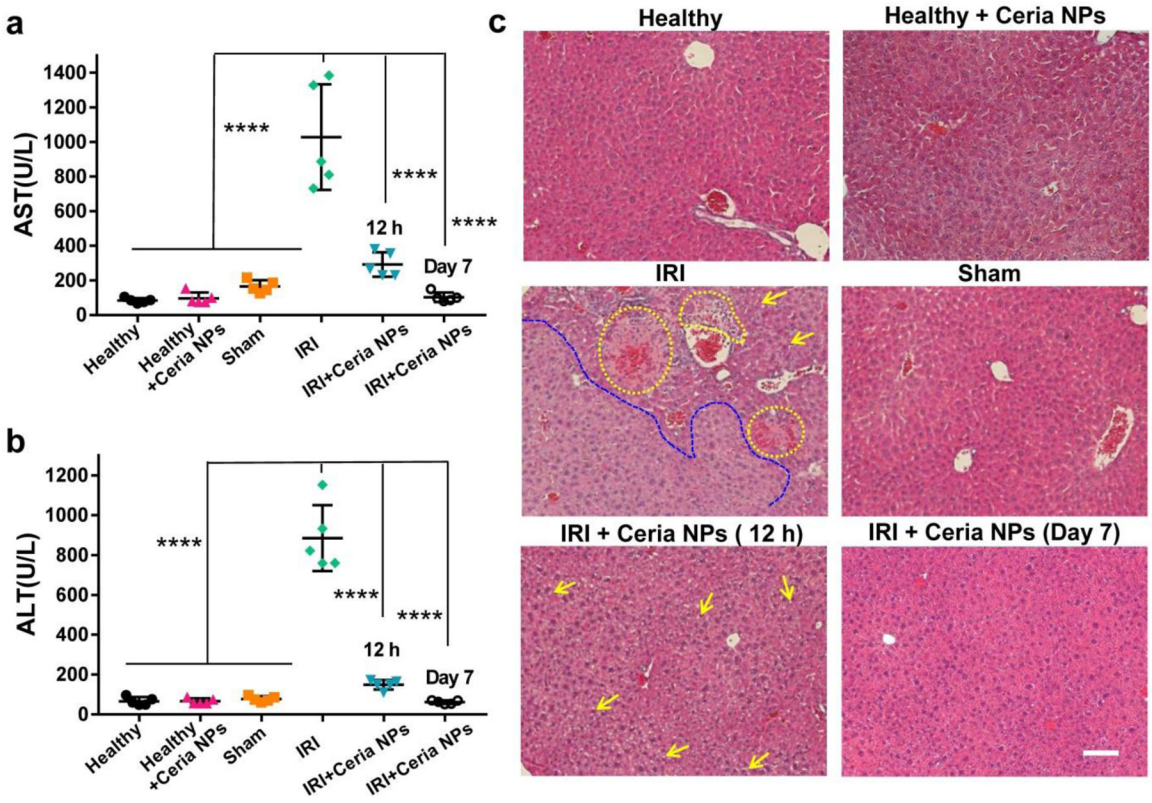

Figure 3. H&E staining and blood serum test after treatment of hepatic IRI.

AST (**a**) and ALT (**b**) levels in blood serum from each group. Lower AST and ALT levels indicate better liver functions. **c** H&E staining of liver tissues from each group. Yellow dash line indicates the hemorrhage as well as cytolysis and necrosis of hepatic cells while the blue dash line showed the severely damaged tissue areas. Yellow arrows indicate the formation of lipid droplets, suggesting mild damaged tissue areas. Scale bar: 100 μm. In **a-b**, data represent means ± s.d. from five independent replicates, and P values were calculated by one-way ANOVA with Tukey's honest significant difference post-hoc test (**** $p < 0.0001$).

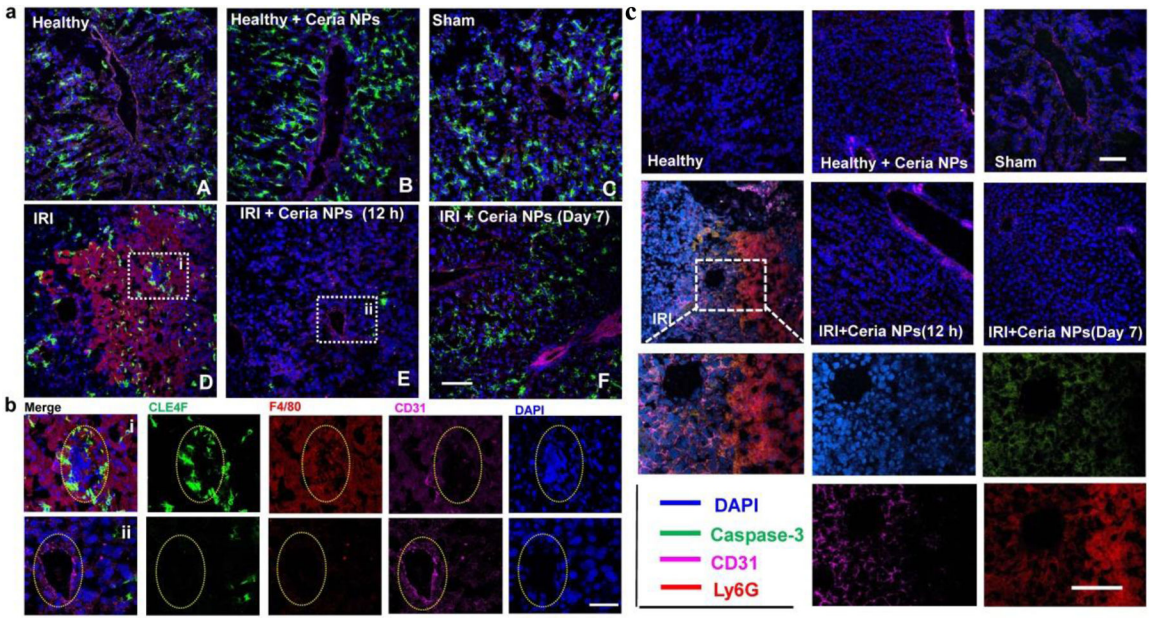

Figure 4. Immunofluorescence staining on liver samples.

a Immunofluorescence staining was performed using anti-CLE4F antibody (green) as Kupffer cell marker, anti-F4/80 antibody (red) as monocyte/macrophage marker, anti-CD31 antibody (pink) as an endothelial marker, and DAPI (blue) for nuclear staining of liver tissues from each group. Scale bar: 100 μm. **b** Enlarged images of immunofluorescence staining in **a** from liver samples of IRI mice treated with PBS (i) or ceria NPs (ii). Scale bar: 50μm. Yellow oval dash line marked the cross-section of blood vessel in liver. **c.** Neutrophil marker was stained by using anti-Ly6G antibody (red), while using anti-caspase-3 antibody (green) as a cell apoptosis marker, anti-CD31 antibody (pink) as an endothelial marker, and DAPI (blue) for nuclear staining of liver tissue from each group. Scale bar: 100 μm.

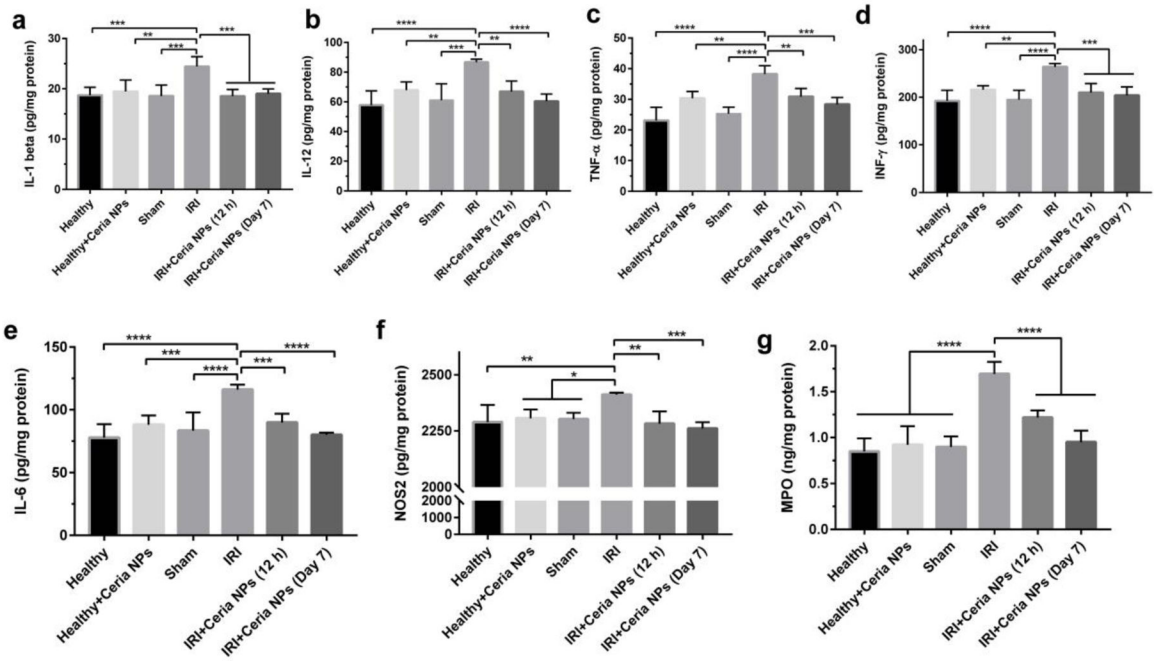

Figure 5. Detection of cytokines in liver tissues.

Cytokines of IL-1 (**a**), IL-12 (**b**), TNF-α (**c**), INF-γ (**d**), IL-6 (**e**), and NOS2 (**f**) from activated monocyte/macrophages and Kupffer cells and MPO (**g**) from activated neutrophil were measured in liver homogenates form each group. Data represent means ± s.d. from five independent replicates, and *P* values were calculated by one-way ANOVA with Tukey's honest significant difference post-hoc (*$p < 0.05$; **$p < 0.01$; *** $p < 0.001$; ****p < 0.0001).

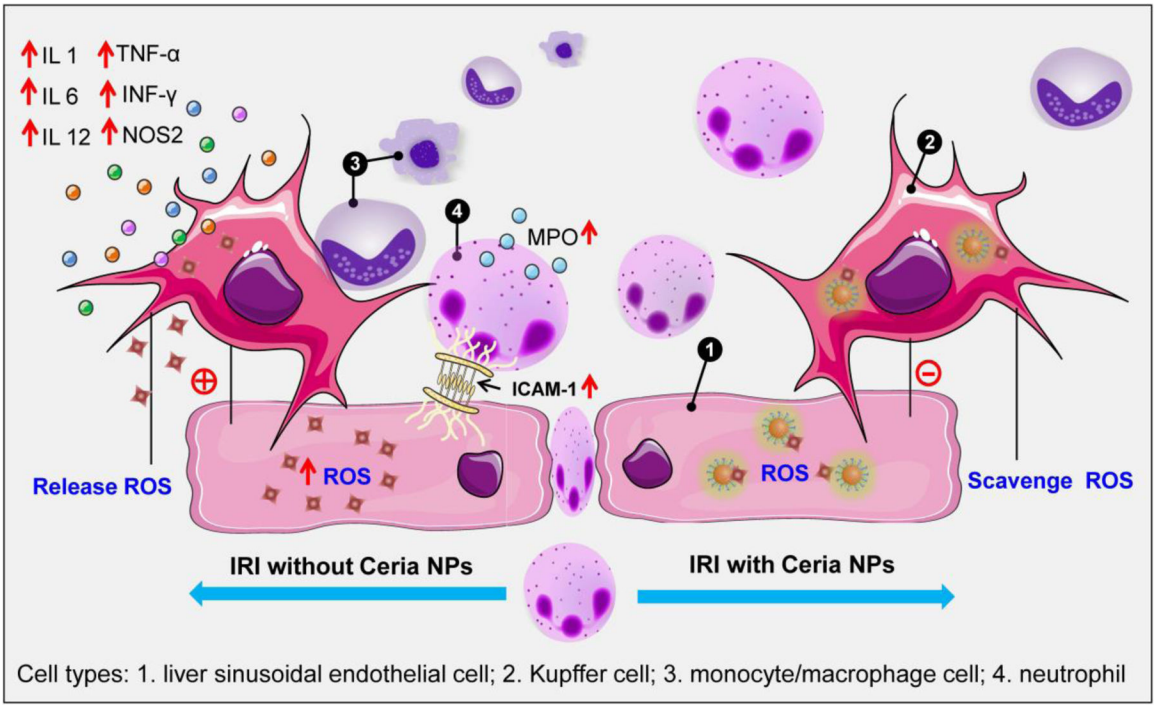

Scheme 1. Mechanism of preventing hepatic IRI by nano-antioxidants.

Ceria NPs can efficiently scavenge ROS from both intracellular (e.g., in the liver sinusoidal endothelial cells and Kupffer cells) and extracellular sources in the liver. As the ROS are neutralized, reduced Kupffer and monocyte/macrophage cells activation limited the release of pro-inflammatory cytokines, which inhibits the recruitment and infiltration of neutrophils. ROS, reactive oxygen species; IL-1, interleukin-1; IL-6, interleukin-6; IL-12, interleukin-12; TNF-α, tumor necrosis factor alpha; INF-γ, interferon gamma; NOS2, nitric oxide synthase 2; ICAM-1, intracellular adhesion molecule-1; MPO, myeloperoxidase.